PAPER

NJC
www.rsc.org/njc

Improved photocatalytic activity of Sn^{4+} doped TiO_2 nanoparticulate films prepared by plasma-enhanced chemical vapor deposition

Yaan Cao,†[a] Wensheng Yang,*[b] Weifeng Zhang,[c] Guozong Liu[b] and Polock Yue*[a]

[a] *Department of Chemical Engineering, Hong Kong University of Science and Technology, Clear Water Bay, Hong Kong, P. R. China*
[b] *College of Chemistry, Jilin University, Changchun 130023, P. R. China. E-mail: wsyang@mail.jlu.edu.cn; Fax: +86-431-8923907; Tel: +86-431-8499234*
[c] *Department of Physics, Hong Kong University of Science and Technology, Clear Water Bay, Hong Kong, P. R. China*

Received* (*in Montpellier, France*) *16th June 2003, Accepted 1st October 2003
First published as an Advance Article on the web 9th December 2003

Sn^{4+} ion doped TiO_2 (TiO_2–Sn^{4+}) nanoparticulate films with a doping ratio of about 7:100 [(Sn):(Ti)] were prepared by the plasma-enhanced chemical vapor deposition (PCVD) method. The doping mode (lattice Ti substituted by Sn^{4+} ions) and the doping energy level of Sn^{4+} were determined by X-ray diffraction (XRD), X-ray photoelectron spectroscopy (XPS), surface photovoltage spectroscopy (SPS) and electric field induced surface photovoltage spectroscopy (EFISPS). It is found that the introduction of a doping energy level of Sn^{4+} ions is profitable to the separation of photogenerated carriers under both UV and visible light excitation. Characterization of the films with XRD and SPS indicates that after doping by Sn, more surface defects are present on the surface. Consequently, the photocatalytic activity for photodegradation of phenol in the presence of the TiO_2–Sn^{4+} film is higher than that of the pure TiO_2 film under both UV and visible light irradiation.

Introduction

TiO_2 has attracted extensive attention due to its effective photodegradation activity for organic pollutants in water and air.[1] So far most of the investigations have focused on preparing TiO_2 catalysts with high photocatalytic activity and TiO_2 catalysts that can be activated by visible light.[2–8] Doping or combining TiO_2 with metal or non-metal ions has been considered as a promising way to improve its photocatalytic activity and enhance its response to visible light.[9–11] Generally, the introduction of doped ions can result in the formation of a doping energy level between the conduction and valence bands of TiO_2, thus making the energy of the transition from the valence band to the doping energy level or from the doping energy level to the conduction band lower than that of the transition from the valence band to the conduction band of TiO_2. In principle, it should be possible for doped TiO_2 to utilize both UV and visible light more efficiently than pure TiO_2 for photocatalytic reactions by introduction of a rationally designed doping energy level in the band gap of TiO_2. Choi *et al.*[12] have studied the effect of different transition metal ion dopants on the oxidation and reduction quantum yields of TiO_2 catalyst and concluded that doping with Fe(III), Mo(V), Ru(III), Os(III), Re(V), V(IV) and Rh(III) at the 0.1–0.5 atom % level in TiO_2 enhanced the photocatalytic activity of catalysts. Recently, the physicochemical properties and photocatalytic activity of TiO_2 doped with Pt, Au, W, Pd, *etc.* were also investigated.[13–18] Yu *et al.*[19] determined the lattice structure of Zr doped TiO_2 and found that its photocatalytic activity was higher than that of pure TiO_2 for the photodegradation of acetone in air. Understanding the mode of doping ions in TiO_2, the effect of doping ions on the lattice and surface structure of TiO_2, the position of the energy level of doping ions in the band gap and their effect on photocatalytic activity will be helpful in designing photocatalysts that give good performance and are sensitive to visible light.

In this work, TiO_2–Sn^{4+} nanoparticulate films were prepared by the plasma-enhanced chemical vapor deposition (PCVD) method. Studied of phenol degradation show that the TiO_2–Sn^{+4} film has a much higher photocatalytic activity than a pure TiO_2 film under both UV and visible light. Based on characterization with X-ray diffraction (XRD), X-ray photoelectron spectroscopy (XPS), surface photovoltage spectroscopy (SPS) and electric field induced surface photovoltage spectroscopy (EFISPS), the doping mode, effect of doping ions on the lattice, surface structure and the doping energy level of Sn^{4+} ions of the TiO_2–Sn^{4+} film are investigated and their effect on the UV and visible light photocatalytic activity of the TiO_2–Sn^{4+} film is discussed.

Experimental

Preparation of the TiO_2–Sn^{4+} film

PCVD is an appropriate technique for preparing thin films of metal oxides doped by metal ions *via* the chemical reaction of the target component plasmas. The reactive precursors for thin film preparation can be ionized by a strong high frequency electric field to form multicomponent plasmas, which will react selectively with each other to form nanoparticles of doped metal oxide, which can be further deposited as thin films. In the process of film growth the reactor is held at a reaction temperature (about 100 °C) much lower than that for conventional chemical vapor deposition (above 900 °C). For the preparation of PCVD deposited TiO_2 thin films, a pressure of 10.6 Pa, power output of 320 W and constant temperature of 110 °C were maintained in the reactor. First, O_2 gas was loaded into reactive chamber at a flow rate of 1 mL min^{-1}. Oxygen

† Present address: College of Physics, Nankai University, Tianjin 300071 P. R. China.

DOI: 10.1039/b306845e

plasmas was obtained in the chamber at a pressure of 40 Pa by high frequency electric field excitation. Subsequently, $TiCl_4$ and $SnCl_4$ were loaded into the reactive chamber at the same time; Ti and Sn plasmas were obtained at a pressure of 66.7 Pa. After 20 min, TiO_2–Sn^{4+} films were obtained on glass slides (7.5×2.5 cm^2). If the deposition time was prolonged to 2 h, TiO_2–Sn^{4+} powder could be acquired. After deposition, $TiCl_4$ and $SnCl_4$ sources were closed down. The films were treated with an O plasma for 10 min, then the substrates coated with the TiO_2–Sn^{+4} film were removed from the reactor, calcined at 450 °C for 30 min and stored in a desiccator before measurements. TiO_2 and SnO_2 films and their powders were prepared by a similar approach under the same conditions.

Characterization of the TiO_2–Sn^{4+} film

XRD patterns of the TiO_2–Sn^{4+}, TiO_2 and SnO_2 powders were acquired by a Rigaku D/max-γA X-ray diffraction spectrometer (CuKα, graphite monochromator). X-Ray photoelectron spectra (XPS) were recorded on a PHI5000 instrument with an Al K_α anode (1486.6 eV). Surface photovoltage spectral (SPS) measurements were carried out with a solid-junction photovoltaic cell of indium tin oxide (ITO)/sample/ITO using a light source, a monochromator, lock-in detection and a computer for collecting data. Monochromatic light was obtained by passing light from a 500 W Xenon lamp through a double-prism monochromator (Higher and Watts, 300). A lock-in amplifier (Brookdeal, 9503-SC), synchronized with a light chopper, was employed to amplify the photovoltage signal.[20] For electric field induced surface photovoltaic spectral (EFISPS) measurements, an electric field is applied to the two electrodes of the photovoltaic cell (ITO/sample/ITO). When its direction is the same as the incident light, the electric field is considered to be positive. Photoluminescence spectra were measured by using the 325 nm line of a He–Cd laser (Omnichrome Products, Melles Griot Laser Group) as excitation source. The experimental setup consists of a monochromator (Model 77200 Oriel Inc.), a photomultiplier tube (Oriel Inc.), an optical chopper (SRS Inc.), a DSP lock-in amplifier (Model SR850, SRS Inc.) and a computer for data processing.

Photocatalytic reaction

The photodegradation of phenol by TiO_2–Sn^{4+} and TiO_2 films was carried out in a 70 ml Pyrex glass reactor. Illumination with $\lambda > 290$ nm was provided by a 400 W high pressure mercury lamp. The films, having an area of 5×2.5 cm^2 and immersed in the solution, were immobilized in the reactor perpendicular to the light beam at a distance of 10 cm from the light source. The phenol solution (5×10^{-5} mol L^{-1}, 40 mL, pH = 5.74) was continuously bubbled by O_2 gas at a flux of 5 ml min^{-1} under magnetic stirring at 25 ± 2 °C. Each hour the residual concentration of phenol was measured by using 4-aminoantipyrine as the chromogenic reagent. For the visible light photocatalytic reaction, a 380 nm filter was employed to remove illumination with $\lambda < 380$ nm provided by a 400 W sunlamp (Philips HPA 400/30 S, Belgium); the concentration of the phenol solution was 3×10^{-5} mol L^{-1}. Other experimental conditions were identical to those used for the UV light photocatalytic reaction. The blank experiment was performed under identical conditions. Distilled water was used in all the experiments and the chemicals were all of analytical grade.

Results and discussion

Fig. 1 shows the X-ray diffraction patterns of the TiO_2 (curve a), SnO_2 (curve b), and TiO_2–Sn^{4+} (curve c) powders prepared by the PCVD method. The TiO_2 and TiO_2–Sn^{4+} samples exhibit an anatase structure while the SnO_2 powder has the rutile structure. After doping, no characteristic peaks of SnO_2 (curve b) were observed in TiO_2–Sn^{4+} (curve c). In the region of 20–80°, the shape of the diffractive peaks of the crystal planes of TiO_2–Sn^{4+} (curve c) is quite similar to that of TiO_2 (curve a), however, the positions of all the diffraction peaks of the TiO_2–Sn^{4+} sample shift to lower diffraction angles compared with those of TiO_2. The diffraction peaks of crystal planes (101), (200) and (105) in curves a and c were selected to determine the lattice parameters and crystallite sizes of the TiO_2 and TiO_2–Sn^{4+} grains, and the peaks of the crystal planes (110), (101) and (211) in curve b were used to calculate those of SnO_2. The lattice parameters and crystallite sizes of the TiO_2, SnO_2 and TiO_2–Sn^{4+} grains are summarized in Table 1. The crystallite size of the TiO_2–Sn^{4+} grains is almost identical to that of TiO_2, while the cell volume and lattice parameters (*a*, *b*, and *c*) of TiO_2–Sn^{4+} increase compared with those of TiO_2.

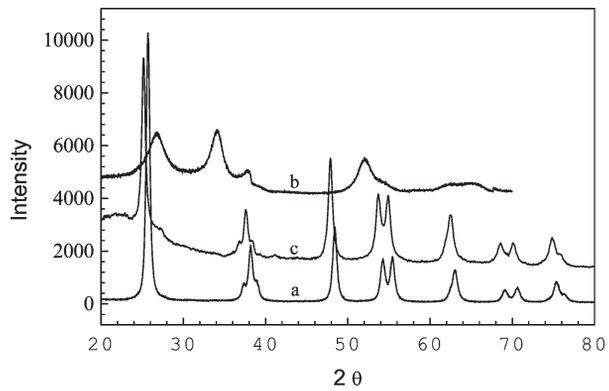

Fig. 1 XRD patterns of the (a) TiO_2, (b) SnO_2 and (c) TiO_2–Sn^{4+} nanoparticulate powders.

It is known that there are two kinds of doping modes, interstitial and substitutional, for doped metal ions in oxides, depending primarily on the electronegativity and ionic radius of the doping metal ions. If the electronegativity and ionic radius of the doping metal ions match those of the lattice metal ion in oxides, the doping metal ion will substitute itself for the lattice metal ion in the doping reactive process (substitutional mode). If the electronegativity of the doping metal ion approaches that of the lattice metal ion and its ionic radius is smaller than that of the lattice metal ion, the oxide lattice spacing will be larger than the ionic radius of the doping metal ions, which will enter into the crystal cell of the oxide (interstitial mode).[21] Since the electronegativity and ionic radius of Sn^{4+} ion (1.8, 69 pm) approach those of Ti^{4+} ion (1.5, 53 pm) in TiO_2,[21] it is expected that the Sn^{4+} ions will replace lattice Ti^{4+} ions and thus occupy lattice Ti^{4+} positions in the doping reactive process. The ionic radius of the doping Sn^{4+} ion is larger than that of the lattice Ti^{4+} ion. This will induce a distortion of the lattice and increment the lattice parameters and cell volume of TiO_2–Sn^{4+} compared with those of TiO_2. As a result, the positions of all the diffraction peaks of TiO_2–Sn^{4+} should shift to lower diffraction angles.

Table 1 Lattice parameters and crystallite sizes of the TiO_2, SnO_2 and TiO_2–Sn^{4+} samples[a]

Sample	a (= b)/Å	c/Å	Cell Volume/Å^3	Crystallite size[b] /Å
SnO_2	4.721	3.179	70.89	90
TiO_2	3.763	9.459	133.9	482
TiO_2–Sn^{4+}	3.813	9.545	137.9	498

[a] The standard deviation of the lattice constants is determined to be <1% as calibrated from the $d_{(111)}$ line of Si. [b] Determined by the Scherrer equation from the line broadening of the XRD patterns.

Fig. 2 shows the Sn $3d_{5/2}$ XPS spectrum of the TiO_2–Sn^{4+} nanoparticulate film. The peak at 486.0 eV is assigned to Sn $3d_{5/2}$ of the doping Sn ions substituting lattice Ti in the film since its position is located between those of Sn $3d_{5/2}$ in SnO_2 (486.5 eV) and Sn $3d_{5/2}$ in metallic Sn (485.0 eV) and the full width half maximum (FWHM) of the peak (2.10) is the same as that of the Sn $3d_{5/2}$ peak of the SnO_2 film prepared by PCVD. The Sn $3d_{5/2}$ and Ti $2p_{3/2}$ XPS spectra of the TiO_2–Sn^{4+} film show that both lattice titanium and doped Sn exist in +4 oxidation states. From the integrated area ratio of the Sn $3d_{5/2}$ and Ti $2p_{3/2}$ peaks, the molar ratio of lattice Ti and doped Sn in the TiO_2–Sn^{4+} film is determined to be about 100:7 after calibration with the response coefficients.

Fig. 3 presents the SPS and EFISPS spectra of the TiO_2 film. In curve a the strong band at 340 nm is attributed to the electronic transition from the valance band to the conduction band of TiO_2. The band threshold at 379 nm corresponds to a band gap of 3.27 eV. Under an external electric field of 0.5 (curve b) and −0.5 V (curve c), no additional peaks are observed, indicating that no extra impurity energy levels can be detected in the band gap. In the SPS and EFISPS spectra of the TiO_2–Sn^{4+} film (Fig. 4), the strong peak at 345 nm (curve a) comes from the transition from the valence band to the conduction band of TiO_2. This response begins at 377 nm, corresponding to a band gap of 3.28 eV. The similar band gaps of the TiO_2 and TiO_2–Sn^{4+} samples indicates that almost no change of the band gap of TiO_2 is induced by Sn^{4+} doping and the TiO_2 and TiO_2–Sn^{4+} films are composed of nanoparticles with almost the same size. It is noted that for the TiO_2–Sn^{4+} film a new weak peak at 430 nm (2.88 eV) is observed, corresponding to a transition below the band gap of TiO_2. Under an external electric field of 0.5 V (curve b), the intensity of this peak decreased, while under an external field of −0.5 V

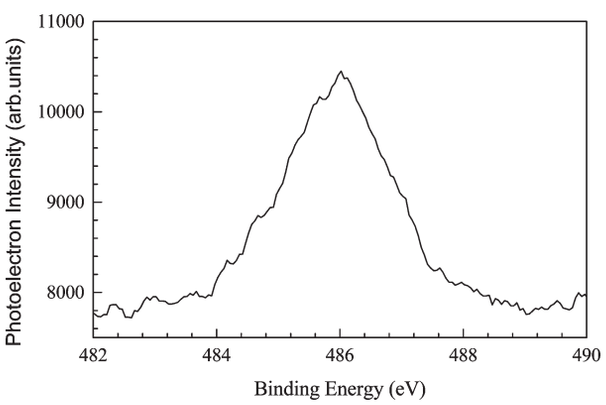

Fig. 2 Sn $3d_{5/2}$ XPS spectrum of the TiO_2–Sn^{4+} nanoparticulate film.

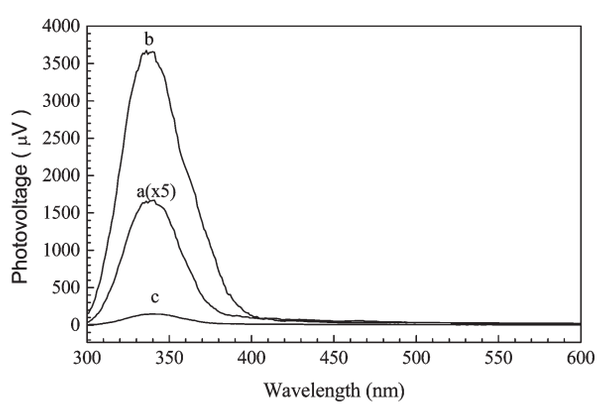

Fig. 3 SPS and EFISPS spectra of the TiO_2 nanoparticulate film with an electric field of (a) 0.0, (b) +0.5 and (c) −0.5 V.

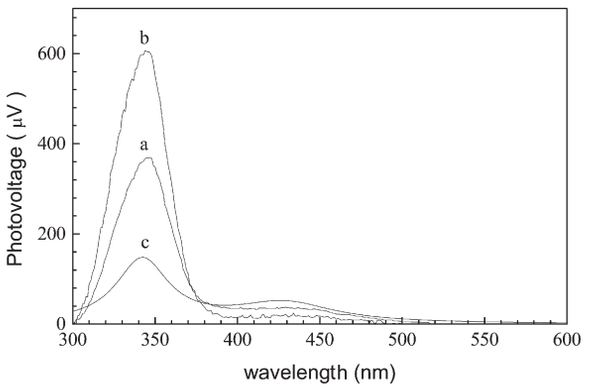

Fig. 4 SPS and EFISPS spectra of the TiO_2–Sn^{4+} nanoparticulate film under an electric field of (a) 0.0, (b) +0.5 and (c) −0.5 V.

(curve c) its intensity increased. This suggests that the peak at 430 nm should be assigned to an electronic transition from the valence band to the doping energy level of the Sn^{4+} ions, which is located 0.4 eV below the conduction band.[22] This assumption is further supported by laser photoluminescence spectral measurements (Fig. 5). For TiO_2–Sn^{4+} (curve b), a new emission peak at 440 nm is detected compared to TiO_2 (curve a). The energy difference of its transition energy (2.82 eV) with the band gap of TiO_2 is about 0.45 eV, consistent with the SPS and EFISPS results. The absence of this peak in curve a suggests this emission should be assigned to the transition from the doping energy level of Sn^{4+} to the valence band of TiO_2.

The effect of Sn doping on the UV and visible light photocatalytic activities of TiO_2 films was evaluated by the photodegradation of phenol. Fig. 6 shows the variation of phenol concentration as a function of photodegradation time under UV (Fig. 6, top) and visible (Fig. 6, bottom) light irradiation. For both TiO_2 and TiO_2–Sn^{4+} films, the $\ln(C_0/C)$ values of phenol show a linear correlation with photodegradation time, suggesting a first-order reaction for both samples. The experimental results of the photodegradation under UV and visible light are illustrated in Tables 2 and 3, respectively. The TiO_2–Sn^{4+} film shows higher photocatalytic activities than the TiO_2 film in both the UV and visible light photocatalytic reactions. The photocatalytic activity of the TiO_2–Sn^{4+} film under UV light is comparable with that of TiO_2/SnO_2 bicomponent films.[6]

In the TiO_2–Sn^{+4} film, some of the lattice Ti in TiO_2 is substituted by Sn^{4+} ions, the cell volume increases and lattice distortion and deformation are induced. This will result in the formation of more structural defects, particularly surface defects,[19] including surface lattice dislocation and coordinatively unsaturated surface cations such as Ti^{4+} and

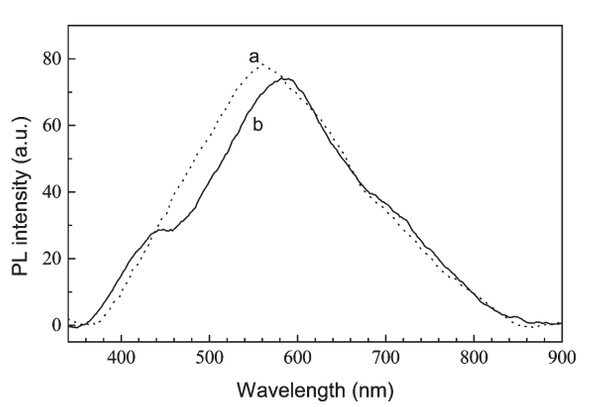

Fig. 5 Laser photoluminescence spectra of the (a) TiO_2 and (b) TiO_2–Sn^{4+} nanoparticulate powders. Excitation wavelength is 325 nm.

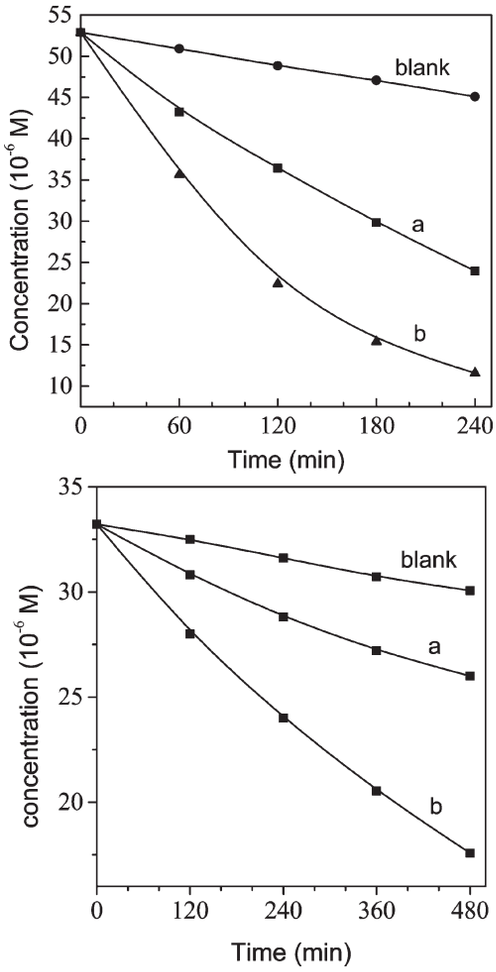

Fig. 6 Variation of phenol concentration with reaction time under (top) UV and (bottom) visible light irradiation. In each plot, curve a corresponds to the TiO_2 film catalyst and curve b corresponds to the TiO_2–Sn^{4+} film catalyst.

Sn^{4+} on the film surface. During the photocatalytic reaction, phenol molecules can be captured by the surface defects on the TiO_2–Sn^{+4} film and are immediately oxidized by photogenerated holes from the valence band of the catalyst.[19] At the same time, these surface defects can efficiently capture O_2 molecules to form O_2^- active species for further photodecomposition of the phenol molecules. The photocatalytic reaction at the solid–liquid interface takes place *via* the following mechanism:

$$O_2(g) + e \rightarrow O_2^-$$
$$O_2^- + 2H^+ + e \rightarrow H_2O_2$$
$$H_2O_2 + e \rightarrow OH^- + OH$$
$$OH^- + h^+ \rightarrow OH$$

Organic pollutants can be further oxidized by active species such as $OH^{\bullet}$ in photocatalytic reactions.[23] As the band-bending direction of TiO_2 is up-and-up at the solid–liquid interface,[24] the photogenerated electrons at the conduction band must experience energy leaping over a potential barrier to reach the surface and be captured by the surface adsorbed O_2 molecules. At the same time, accumulated photogenerated electrons at the bottom of the bent conduction band will increase the probability of electron–hole recombination during the photocatalytic reaction. After Sn doping, since the doping energy level of Sn^{4+} ions is located 0.4 eV (NHE 0.2 eV) below the conduction band, which is higher than the electrode potential of O_2/H_2O_2 (NHE 0.34 eV), photogenerated electrons on the particle surface generated by visible light at the doping energy level of the Sn^{4+} ions can be captured directly by the efficiently adsorbed O_2 molecules on the TiO_2–Sn^{4+} surface. In the case of UV light, the photogenerated electrons at the conduction band can be transferred to the doping energy level of the Sn^{4+} ion and can then be captured by absorbed O_2 molecules on the TiO_2–Sn^{4+} surface. This will accelerate the separation of photogenerated holes and electrons, prohibiting their recombination. As a result, more photogenerated electrons and holes contribute to the photocatalytic reaction, improving the photocatalytic activitives under both UV and visible light.

Conclusion

A TiO_2–Sn^{4+} nanoparticulate film prepared by PCVD shows higher photocatalytic activity than the pure TiO_2 film under both UV and visible light irradiation. The doping of Sn^{4+} results in more surface defects, allowing the more effective absorption of both phenol and O_2. The doping energy level of Sn^{4+} ions approaches the conduction band of TiO_2 and allows the photogenerated electrons to be transferred more efficiently to the surface *via* the doping energy level. The doping of Sn can promote the separation of photogenerated

Table 2 Photodegradation of phenol with TiO_2 and TiO_2–Sn^{4+} films under UV illumination

Sample	Film weight/mg	Phenol degraded[a] $(C_0 - C)/C_0$	k^b/min^{-1}	$t_{1/2}$/min	Specific photocatalytic activity/mol g^{-1} h^{-1}
Blank[c]	–	0.037	5.60×10^{-4}	1245.9	–
A (TiO_2)	0.81	0.204	3.80×10^{-3}	182.0	4.80×10^{-4}
B (TiO_2–Sn^{4+})	0.83	0.326	6.17×10^{-3}	112.3	8.30×10^{-4}

[a] After reaction for 1 h. [b] Apparent rate constant deduced from the linear fitting of $\ln(C_0/C)$ *versus* reaction time. [c] The blank was a 5×2.5 cm^2 glass slide without any catalyst.

Table 3 Photodegradation of phenol with the TiO_2 and TiO_2–Sn^{4+} films under visible light

Sample	Film weight/mg	Phenol degraded[a] $(C_0 - C)/C_0$	k^b/min^{-1}	$t_{1/2}$/min	Specific photocatalytic activity/mol g^{-1} h^{-1}
Blank[c]	–	0.021	2.13×10^{-4}	3246.6	–
A (TiO_2)	0.81	0.072	5.12×10^{-4}	1353.8	5.90×10^{-5}
B (TiO_2–Sn^{4+})	0.83	0.156	1.25×10^{-3}	554.5	1.24×10^{-4}

[a] After reaction for 2 h. [b] Apparent rate constant deduced from the linear fitting of $\ln(C_0/C)$ *versus* reaction time. [c] The blank was a 5×2.5 cm^2 glass slide without any catalyst.

carriers under both UV and visible light irradiation. More precise control over the lattice and surface structure of doped TiO_2 and the energy level of doping ions in the band gap will be helpful to prepare TiO_2 photocatalysts that are more sensitive to both UV and visible light irradiation.

Acknowledgements

This work is supported by the National Natural Science Foundation of China, Hong Kong Research Grant's Council (HKUST 6247/00P) and the Excellent Young Teachers Program of MOE, P. R. C.

References

1 A. L. Linsebigler, G. Lu and J. T. Yates, *Chem. Rev.*, 1995, **95**, 735.
2 I. Sopyan, M. Watanabe, S. Murasawa, K. Hashimoto and A. Fujishima, *Chem. Lett.*, 1996, 69.
3 S. Deki, Y. Aoi, O. Hiroi and A. Kajinami, *Chem. Lett.*, 1996, 433.
4 K. Vinodgopal, I. Bedja and P. V. Kamat, *Chem. Mater.*, 1996, **8**, 2180.
5 K. Y. Song, M. K. Park, Y. T. Kwon, H. W. Lee, W. J. Chung and W. I. Lee, *Chem. Mater.*, 2001, **13**, 2349.
6 Y. A. Cao, X. T. Zhang, W. S. Yang, H. Du, Y. M. Chen, Y. B. Bai, T. J. Li and J. N. Yao, *Chem. Mater.*, 2000, **12**, 3445.
7 A. Dawson and P. V. Kamat, *J. Phys. Chem. B.*, 2001, **105**, 960.
8 R. Asahi, T. Morikawa, T. Ohwaki, K. Aoki and Y. Taga, *Science*, 2001, **293**, 269.
9 X. Z. Li and F. B. Li, *Environ. Sci. Technol.*, 2001, **35**, 2381.
10 V. Subramanian, E. Wolf and P. V. Kamat, *J. Phys. Chem. B.*, 2001, **105**, 11 439.
11 K. Rajeshwar, N. R. De Tacconi and C. R. Chenthamarakshan, *Chem. Mater.*, 2001, **13**, 2765.
12 W. Choi, A. Termin and M. R. Hoffmann, *J. Phys. Chem.*, 1994, **98**, 13 669.
13 C. Y. Wang, C. Y. Liu, J. Chen and T. Shen, *J. Colloid Interface Sci.*, 1997, **191**, 464.
14 C. Y. Wang, C. Y. Liu, X. Zheng, J. Chen and T. Shen, *Colloid. Surf., A*, 1998, **131**, 271.
15 A. Sclafani, L. Palmisano, G. Marcí and A. M. Venezia, *Sol. Energy Mater. Sol. Cells*, 1998, **51**, 203.
16 J. C. Yang, Y. C. Kim, Y. G. Shul, C. H. Shin and T. K. Lee, *Appl. Surf. Sci.*, 1997, **121/122**, 525.
17 M. M. Rahman, K. M. Krishna, T. Soga, T. Jimbo and M. Umeno, *J. Phys. Chem. Solids*, 1999, **60**, 201.
18 K. M. Krishna, M. Mosaddeq-ur-Rahman and T. Miki, *Appl. Surf. Sci.*, 1997, **113/114**, 149.
19 J. C. Yu, J. Lin and R. W. M. Kwok, *J. Phys. Chem. B.*, 1998, **102**, 5094.
20 D. J. Wang, J. Zhang, T. S. Shi, B. H. Wang, X. Z. Cao and T. J. Li, *J. Photochem. Photobiol. A: Chem.*, 1996, **93**, 21.
21 Y. L. Xu, *The Basics of Semiconducting Oxides and Compounds*, Press of Xi'an Electronic Science and Technology University, Xi'an, 1991.
22 L. Kronik and Y. Shapira, *Surf. Sci. Rep.*, 1999, **37**, 1.
23 M. R. Hoffmann, S. T. Martin and D. W. Bahnemann, *Chem. Rev.*, 1995, **95**, 69.
24 M. Anpo, K. Chiba, M. Tomonari, S. Coluccia, M. Che and M. A. Fox, *Bull. Chem. Soc. Jpn.*, 1991, **64**, 543.